Lattice Dynamics of Sb$_2$Se$_3$ from Inelastic Neutron and X-Ray Scattering

Markus G. Herrmann, Ralf P. Stoffel, Ilya Sergueev, Hans-Christian Wille, Olaf Leupold, Mohammed Ait Haddouch, Gabriele Sala, Doug L. Abernathy, Jörg Voigt, Raphaël P. Hermann, Richard Dronskowski, and Karen Friese*

The lattice dynamics of orthorhombic Sb$_2$Se$_3$ is studied by a combination of inelastic neutron and ^{121}Sb nuclear inelastic scattering giving access to the total and Sb partial density of phonon states (DPS). The Se partial DPS is determined from the difference between the total and Sb partial DPS. The total DPS is determined at 39, 150, and 300 K, and an analysis of the temperature-induced mode shifts in combination with low-temperature powder diffraction data is provided. Using an earlier reported theoretical approach, the corresponding total and partial DPS of Sb$_2$Se$_3$ are calculated by first-principles calculations. Herein, a detailed analysis of the Grüneisen parameter, element-specific and bulk Debye temperatures, and the mean force constants as derived from the experimental data and discrete Fourier transform calculations is provided. In general, the calculations underestimate the strength of the covalent Sb—Se bonds.

1. Introduction

The semiconductor antimony sesquiselenide, Sb$_2$Se$_3$, has attracted attention because the material is a promising candidate for several applications in energy and data storage devices. Sb$_2$Se$_3$ has a bandgap of around 1.1–1.2 eV and a high absorption coefficient of $>10^5$ cm^{-1} for visible light which makes it a potential absorber material in solar cells.[1,2] Moreover, the compounds in the Sb$_2$Se$_3$–Sb$_2$Te$_3$ solid solution as well as Sb$_2$Se$_3$ thin films exhibit phase-change properties.[3,4] Phase-change materials (PCM) are characterized by an ultrafast and reversible temperature-induced phase transition between an amorphous and a crystalline phase, which is accompanied by a pronounced contrast between the electrical, optical, and thermal properties of both phases.[3,4] Therefore, Sb$_2$Se$_3$ is considered to be a promising material for future PCM-based data storage.

The crystal structure of antimony sesquiselenide (Sb$_2$Se$_3$) (space group *Pnma*; $a = 11.7938(9)$ Å, $b = 3.9858(6)$ Å, $c = 11.6478(7)$ Å[5]) is characterized by covalently bonded —Se—Sb—Se— chains arranged along the [010] direction (**Figure 1**).[5] Two symmetry-independent Sb (Sb1 and Sb2) and three Se (Se1, Se2, and Se3) positions exist in the structure in which all atoms occupy Wyckoff position $4c$ (x, 1/4, z; site symmetry m). Moreover, several van der Waals interactions have been identified in the crystal structure of Sb$_2$Se$_3$.

Based on first-principles calculations,[6] several intra- and interchain interactions were postulated for Sb$_2$Se$_3$. The total and element-specific density of phonon states (DPS) and a detailed mode analysis were also predicted; however, an experimental validation for the predicted phonon data is missing yet. The theoretically determined cutoff frequency of Sb$_2$Se$_3$ (≈ 25 meV) was compared with the ones reported for other Sb$_2X_3$ ($X = $ S, Te) chalcogenides, and it was found that Sb$_2$Se$_3$ is harder than Sb$_2$Te$_3$ (≈ 21 meV[7]), but significantly softer than Sb$_2$S$_3$ (≈ 40 meV[8]).

Dr. M. G. Herrmann, M. Ait Haddouch, Dr. J. Voigt, Dr. K. Friese
Jülich Centre for Neutron Science-2/Peter Grünberg Institute-4
Forschungszentrum Jülich GmbH
Wilhelm-Johnen Strasse, Jülich 52428, Germany
E-mail: k.friese@fz-juelich.de

Dr. R. P. Stoffel, Prof. R. Dronskowski
Chair of Solid-State and Quantum Chemistry
Institute of Inorganic Chemistry
RWTH Aachen University
Landoltweg 1, Aachen 52056, Germany

Dr. I. Sergueev, Dr. H.-C. Wille, Dr. O. Leupold
Photon Science (FS)
Deutsches Elektronen-Synchrotron (DESY)
Notkestrasse 85, 22607 Hamburg, Germany

Dr. G. Sala, Dr. D. L. Abernathy
Neutron Scattering Division
Oak Ridge National Laboratory
Oak Ridge, TN 37831, USA

Dr. R. P. Hermann
Materials Science and Technology Division
Oak Ridge National Laboratory
Oak Ridge, TN 37831, USA

Prof. R. Dronskowski
Hoffmann Institute of Advanced Materials
Shenzhen Polytechnic
7098 Liuxian Blvd, Nanshan District, Shenzhen 518055, China
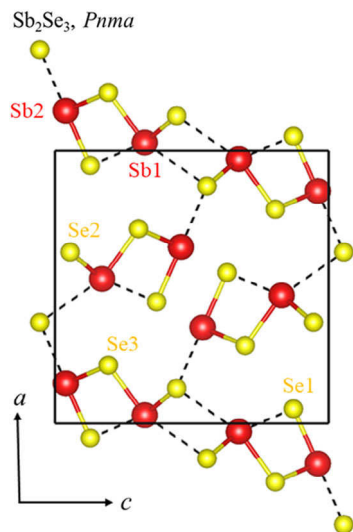
Figure 1. Projection of the Sb_2Se_3 structure[5] on the ac plane. The different Wyckoff positions are labeled.

Figure 2. Temperature dependence of the normalized lattice parameter of Sb_2Se_3. Lattice parameters at 300 K are the following: $a = 11.7752(7)$ Å, $b = 3.9749(2)$ Å, $c = 11.6255(5)$ Å.

Low-temperature heat capacity measurements on Sb_2Se_3 yielded a macroscopic Debye temperature of 177.1(4) K.[9] Although the cutoff energy characterizes the energy of the energetically highest phonon branch, the Debye energy (which is related to the Debye temperature, θ_D, via $E_D = k_B \cdot \theta_D$; k_B: Boltzmann constant) defines the energy at which the integrals of the experimental and Debye DPS ($G(E)_D \sim E^2$; E: phonon energy) are equal.

Herein, the lattice dynamics of Sb_2Se_3 was investigated by combining inelastic neutron scattering (INS) and ^{121}Sb nuclear inelastic scattering (NIS) measurements from which the total and Sb partial DPS were determined. The Se DPS was then deduced from the difference between the total and Sb DPS. A detailed analysis of the temperature-induced mode shifts of Sb_2Se_3 is presented on the basis of the total DPS which we have determined at 39, 150, and 300 K. Low-temperature powder diffraction data allow the estimation of the Grüneisen parameter of several modes. Element-specific Debye temperatures and mean force constants were derived from our phonon data. The experimental data are supported by first-principles calculations.

2. Results and Discussion

The temperature dependence of the normalized lattice parameters of Sb_2Se_3 is shown in **Figure 2**. Based on our low-temperature X-ray powder diffraction (XRD) measurements, we found that the orthorhombic phase of Sb_2Se_3 is stable down to at least 40 K as we did not observe any hints for phase transitions. All lattice parameters show a very similar low-temperature behavior and an exclusively positive thermal expansion between 40 and 300 K. The normalized lattice parameter a_i/a_{300} shows the smallest temperature-induced change, whereas b_i/b_{300} and c_i/c_{300} are slightly more affected by the temperature. From the diffraction data, we have determined direction-dependent thermal expansion coefficients of $\alpha_a = 1.12(4) \times 10^{-5}$ K^{-1}, $\alpha_b = 1.19(6) \times 10^{-5}$ K^{-1}, and $\alpha_c = 1.35(3) \times 10^{-5}$ K^{-1} and a volume thermal expansion coefficient of $\alpha_V = 3.7(1) \times 10^{-5}$ K^{-1} between 40 and 300 K using
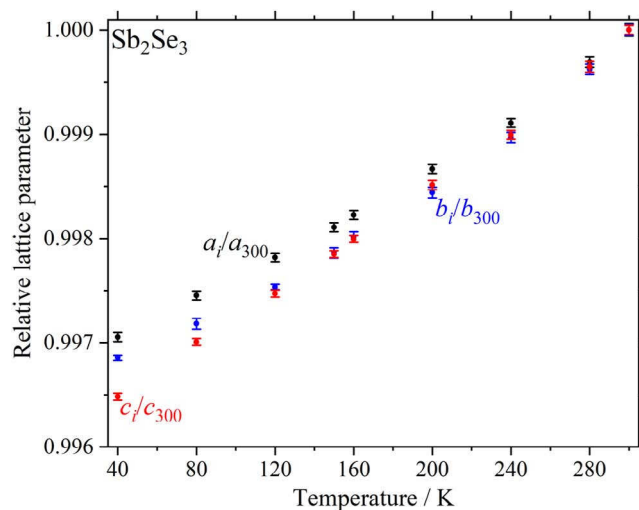
the relation $\alpha_i = [da_i/dT]/a_{300}$ where $[da_i/dT]$ represents the derivative of lattice parameter a_i and a_{300} is the value of the corresponding lattice parameter at 300 K. Along the [100] and [010] direction, we found nearly identical thermal expansion coefficients, whereas the one derived from the c lattice parameter is slightly larger. The anisotropic thermal expansion of Sb_2Se_3 indicates that the weaker intra- and interchain interactions mainly contribute to the [001] direction, whereas the contribution of these interactions to the other directions is smaller. However, to further investigate the distribution of the different bonding in the crystal structure of Sb_2Se_3 (temperature-dependent), single-crystal data are required.
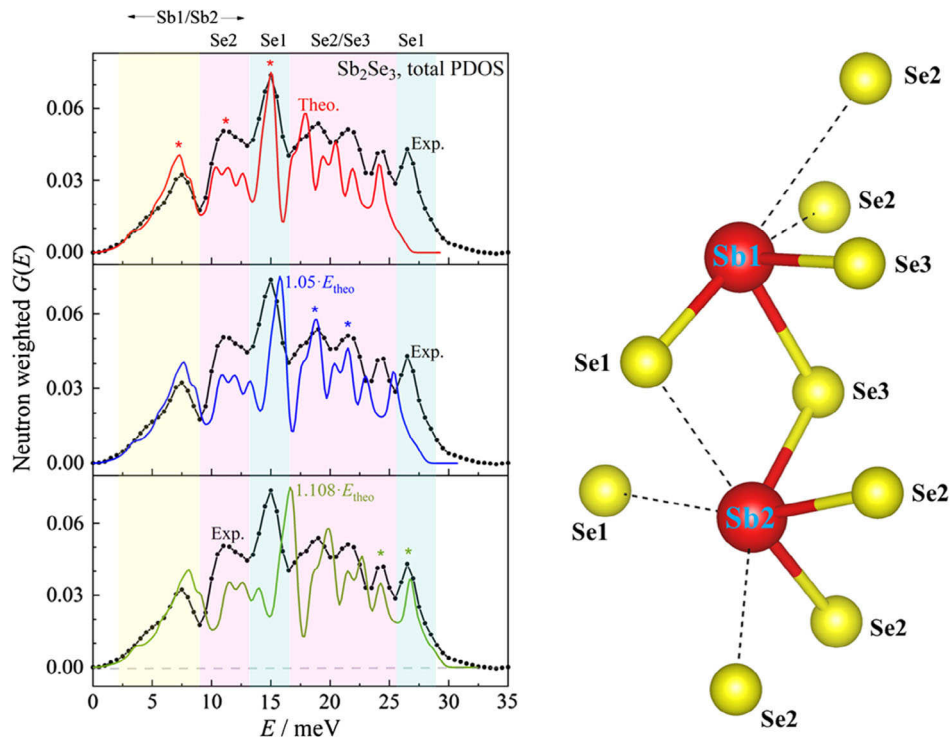
The total DPS of Sb_2Se_3 determined experimentally and obtained from first-principles calculations is shown in **Figure 3** (the ^{121}Sb and Se partial DPS are shown in **Figure 4**). To allow for an easier comparison of the results, the amplitude, I(DPS), of the theoretically predicted DPS was scaled to the experimental one by $\varepsilon_1 \cdot I$(DPS), where ε_1 is a fictive scaling factor. For Sb_2Se_3, an experimental cutoff energy of around 32 meV was found. The compound is therefore harder than Sb_2Te_3 ($\approx$21 meV) but softer than Sb_2S_3 ($\approx$40 meV). Thus, our experimental data support the conclusion of a previous study.[6]

The temperature-dependent isochoric heat capacity of Sb_2Se_3 was calculated from the measured total DPS using Equation (1)

$$c_V(T) = 3 \cdot n \cdot R \cdot \int_0^{C.E.} G(E) \cdot \frac{x^2 \cdot \exp(x)}{(\exp(x) - 1)^2} \, dE \quad (1)$$

where n is the number of oscillators, R is the universal gas constant, $G(E)$ is the total DPS, and $x = E/k_B \cdot T$ ($k_B =$ Boltzmann constant).[10] An integration was performed up to the cutoff energy of 32 meV (C.E. = cutoff energy). The obtained heat capacity data were fitted with the Debye model[10] (Equation (2))

$$c_V(T) = 9 \cdot n \cdot R \cdot \left(\frac{T}{\theta_{D,INS}}\right)^3 \int_0^{\theta_{D,NIS}/T} \frac{x^4 \cdot \exp(x)}{(\exp(x) - 1)^2} \, dE \quad (2)$$

ADVANCED
SCIENCE NEWS
www.advancedsciencenews.com

physica
pss status solidi b
www.pss-b.com

Figure 3. Left: Total DPS of Sb_2Se_3 measured (black line dots) and calculated (colored lines). Scaling factors of 1.05 (middle) and 1.108 (bottom), respectively, were applied to the theoretical data. Right: Fragment of the Sb_2Se_3 structure adapted from ref. [5] in which the different Wyckoff positions are labeled. The energy ranges in which atoms at given Wyckoff position dominate the DPS of Sb_2Se_3 correspond to the ones from ref. [6] and are marked in the phonon data.
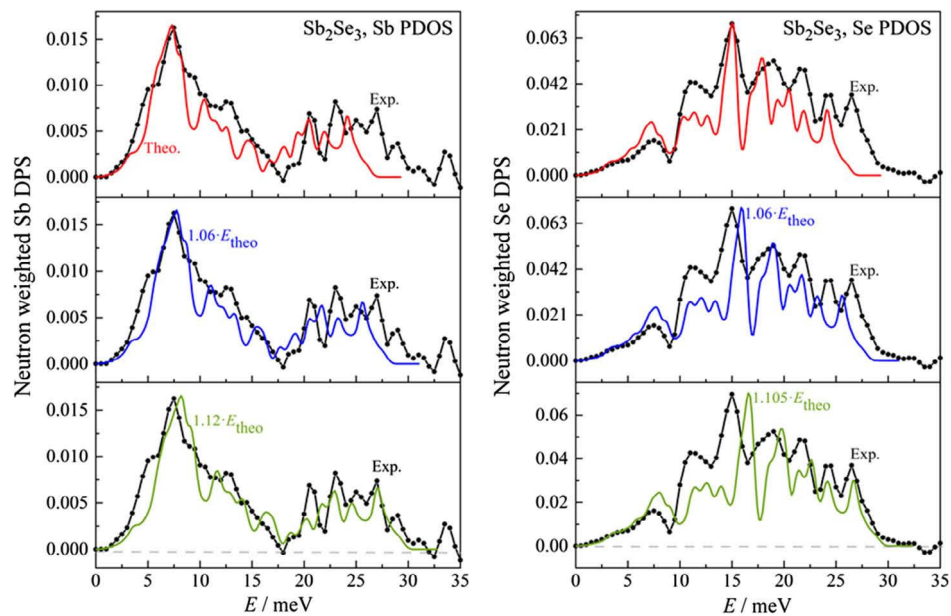
Figure 4. Sb and Se partial DPS of Sb_2Se_3 derived from the INS and NIS data and obtained from the first-principles calculations. Scaling factors (middle, bottom) were applied to achieve an overlap between experimental and theoretical phonon data in the high-energy range ($E > 15$ meV).

We found a macroscopic Debye temperature of $\theta_{D,INS} = 233(3)$ K, which is significantly larger than the value presented by Herrmann et al.[9] (177.1(4) K).

From our ^{121}Sb NIS experiment, we have determined the values of 0.47(1) for the Lamb–Mössbauer factor and 120(6) N m^{-1} for the mean force constant, respectively. A mean force constant of

ADVANCED
SCIENCE NEWS
www.advancedsciencenews.com

physica **pss** b
status solidi
www.pss-b.com

100(6) N m^{-1} was calculated for Se from the area weighted DPS, $g(E)$, using Equation (3)

$$\phi_i = M_i \cdot \int_0^\infty \frac{g(E) \cdot E^2}{\hbar^2} \mathrm{d}E \qquad (3)$$

where M_i is the element mass and $\hbar$ corresponds to the reduced Planck constant. The theoretical force constants $\Phi_{ij\alpha\beta}$ are accessible from the forces $F_{i\alpha}$ and a displacement $d_{j\beta}$ (i and j stand for two individual atoms, whereas α and β indicate the Cartesian directions x, y and z) via the relation

$$F_{ij\alpha\beta} = -F_{i\alpha}/d_{j\beta} \qquad (4)$$

As already discussed by Stoffel et al.,[7] the averaged force constants $\bar{\Phi}$ for each atom resulting from their own displacements in the same direction as the forces (therefore, $i = j$ and $\alpha = \beta$ in Equation (4)) can be directly compared with the experimentally determined ones (**Table 1**). In general, the experimental and theoretical Sb mean force constants provide slightly larger values compared with the Se data. The theoretical averaged force constants of antimony are smaller than the experimental value by ≈25%, whereas for Se we found deviations between about 12% and 20%.

In addition, we have predicted the directionally resolved mean force constant for each symmetry-independent atom to quantify the anisotropy of the bond strength in Sb$_2$Se$_3$. Obviously, the largest mean force constants are found along the [100] direction, whereas, in the [010] direction, the smallest values occur; therefore, it is indicated that the strongest and weakest Sb—Se bonds occur along this direction, respectively. Moreover, we found that the directionally resolved force constants of both elements in the x direction are much closer to the experimental values. For selenium, this effect is much stronger than for antimony.

Element-specific Debye temperatures, $\theta_{D,i}$, were calculated from the partial Sb and Se DPS using Equation (5)

$$\theta_{D,i} = \left(\frac{3}{k_B^2 \cdot \int_0^{C.E.} g(E)\mathrm{d}E/E^2} \right)^{\frac{1}{2}} \qquad (5)$$

where k_B is the Boltzmann constant, $g(E)$ is the respective partial DPS, and C.E. represents the cutoff energy. We found Debye temperatures of $\theta_{D,Sb} = 160(6)$ K and $\theta_{D,Se} = 239(6)$ K for Sb and Se, respectively. As expected from their masses, the Debye temperature of Se is larger than the one of Sb. Using

the same procedure, we have also calculated the element-specific Debye temperatures from the theoretically predicted Sb and Se DPS as shown in Figure 4. We found the theoretical Debye temperatures of $\theta_{D,Sb} = 141.57$ K and $\theta_{D,Se} = 189.23$ K. The theoretically predicted Sb Debye temperature slightly underestimates the corresponding experimental value, whereas for Se theory underestimates the Debye temperature more clearly. To explain the origin of these deviations, we provide a detailed analysis of our experimentally determined and theoretically predicted total and partial DPS in the following.

According to the results of a previous study,[6] the modes in the low-energy range between about 0 and 10 meV in both the experimental and theoretical DPS are dominated by Sb, whereas energetically higher lying modes are dominated by Se. Due to the limited resolution, the experimental data show fewer features than the theoretical ones. The comparison shows that, between 0 and 15 meV, the experimentally determined and theoretically predicted mode energies are in very good agreement, whereas their intensities differ significantly (especially between 6 and 10 meV). At higher energies, a pronounced mismatch between theory and experiment is clearly visible both in the total and partial DPS (Figure 3 and 4).

To better understand the deviations between the experimental and theoretical data, we have scaled the mode energies of the theoretically determined DPS to the experimental one by applying a fictive scaling factor $\varepsilon_2 \cdot E(\text{DPS})$. It is important to mention that our scaling ignores the conversion of the norm of the theoretical DPS (which would be given by $\varepsilon_2 \cdot E(\text{DPS})$ with $\frac{1}{\varepsilon_1} \cdot I(\text{DPS})$ and $\varepsilon_1 = \varepsilon_2$). This is, as we selected the same scaling for the intensities of the theoretical DPS as introduced earlier for all of the following analysis ($\varepsilon_1 = \varepsilon_2$ is not necessarily given) to ease the understanding of our statements.

Initial energy-scaling factors were derived from the ratio between the lattice parameters determined in this study at 40 K (which corresponds to the same temperature at which we have measured our NIS data) and the corresponding data delivered in the study by Deringer et al.[6] (**Table 2**). A scaling factor of 1.05—comparable with the ratio of experimentally and theoretically determined unit cell volumes (Table 2)—leads to an overlap in the energy range between 15 and 25 meV, whereas the ratios of the individual lattice parameters a, b, c are too small to gain a sufficient overlap in this energy range. To produce an overlap of the modes at higher energies of the total DPS, a larger scaling factor of 1.108 (1.12 for Sb DPS; 1.105 for Se DPS) must be used. As this factor is significantly larger than those derived from the difference in unit cell volumes and in lattice parameters, respectively, we assume that the

Table 1. Experimental and theoretical atomic force constants of Sb$_2$Se$_3$. $\bar{\Phi}$ is the average force constant and $\Phi_{x,y,z}$ are the directionally resolved ones.

Atom	$\bar{\Phi}_{exp}$ [N m^{-1}]	$\bar{\Phi}_{theo}$ [N m^{-1}]	Φ_x [N m^{-1}]	Φ_y [N m^{-1}]	Φ_z [N m^{-1}]
Sb1	120(6)	87.3	94.8	96.3	70.8
Sb2		92.6	111.9	81.0	85.0
Se1		82.2	109.4	64.0	73.4
Se2	100(6)	79.8	81.6	80.1	77.8
Se3		88.1	97.2	71.3	95.7

Table 2. Lattice parameter of Sb$_2$Se$_3$ derived from the low-temperature powder diffraction measurements (40 K), and theory[6] and their ratios (denoted as "E_{exp}/E_{theo}").

	This study	Ref. [6]	E_{exp}/E_{theo}
a [Å]	11.7405(5)	11.534	1.018
b [Å]	3.9624(1)	3.960	1.001
c [Å]	11.5846(4)	11.221	1.032
V [Å^3]	539.92(5)	512.52	1.052

applied theoretical approach underestimates the bond strength of at least some of the covalent Sb—Se bonds. This is supported by the fact that most of the predicted bond lengths of the covalent Sb—Se bonds[6] are significantly longer than the corresponding experimental values.[5] Unfortunately, total and partial DPS calculated from experimental lattice parameters and bond lengths provided phonon data with a significant imaginary contribution which clearly indicates that the structural model is unstable with respect to the underlying methodology. Therefore, a more detailed analysis of the bond strength in the theoretical and experimental structure is not possible.

The total DPS of Sb_2Se_3 was measured at 39, 150, and 300 K (**Figure 5**). The comparison shows that all phonon modes soften with increasing temperature, as expected, as the thermal movement of the atoms increases, resulting in a weakening of the Sb—Se bonds and Sb—Se interactions.

To accurately determine the peak positions of the modes highlighted in Figure 4, we have fitted our experimental data with a series of Gaussian functions (Figure S2, Supporting Information). In Figure S3, Supporting Information, the extracted mode energies are plotted depending on the unit cell volumes which were obtained from our low-temperature powder diffraction study. We have subsequently applied linear fits to the data in Figure S3, Supporting Information, to determine the slope $\frac{\delta E}{\delta V}$ (**Table 3**). From these values, we have determined the Grüneisen parameters γ_i ($\gamma_i = \frac{V_{300}}{E_{300}} \cdot \frac{\delta E}{\delta V}$; V, V_{300}, E, E_{300}: unit cell volume/mode energy at temperature T, 300 K; $\frac{\delta E}{\delta V}$ slope) in Figure S2, Supporting Information, of all modes which are shown in Table 3. In Figure S4, Supporting Information, we show the energy-dependent changes of the Grüneisen parameter of all vibrational modes which we have determined from our discrete Fourier transform calculations. In general, the calculated Grüneisen parameter decreases with the increasing mode energy. In Table 3, we compare our theoretical γ_i values to the experimental ones. Obviously, the experimentally determined Grüneisen parameter of the two energetically lowest-lying modes fit nicely to the theoretical data, whereas for all energetically higher-lying modes we observed pronounced deviations

Table 3. Experimental mode energies ($E_{exp.}$) and their volume-dependent changes ($\delta E/\delta V$) as derived from Figure S3, Supporting Information, from which the Grüneisen parameter (γ_{exp}) was determined. Theoretical Grüneisen parameters ($\gamma_{theo.}$) are shown for comparison. Error bars in E_{exp} and $\delta E/\delta V$ were taken from the fits shown in Figure 3 and 4, respectively.

| E_{exp} [meV]	$\delta E/\delta V$ [meV Å^{-3}]	$\gamma_{exp.}$	$\gamma_{theo.}$
7.34(17)	−0.043(2)	3.19(17)	3.0
11.28(20)	−0.041(23)	2.0(12)	1.9
14.77(19)	−0.020(8)	0.74(30)	2.1
18.35(18)	−0.068(12)	2.0(36)	0.6
21.57(19)	−0.084(18)	2.1(45)	0.6
23.63(19)	−0.114(7)	2.6(17)	0.1
26.09(19)	−0.075(17)	1.6(36)	0.01

between the experimental and theoretical data. At this point, it is important to re-emphasize that in our theoretical approach the thermal expansion of the unit cell is considered by an expansion of the simulation cell at 0 K and, therefore, the Sb—Se bond lengths remain constant over the entire temperature range. Therefore, the discrepancy between the experimentally and theoretically determined Grüneisen parameter might be due to the temperature-induced changes of the Sb—Se bond lengths, which are only present in our experimental data.

3. Conclusions

The lattice dynamics of Sb_2Se_3 was investigated by a combination of XRD, INS and NIS measurements, and first-principles calculations. The low-temperature behavior of Sb_2Se_3 was studied by powder diffraction measurements for the first time. The material shows an exclusively positive thermal expansion and an anisotropy along the [001] direction. We assume that this is caused by the higher contribution of weaker intra- and interchain interactions in this direction. However, based on our neutron data, we did not observe any anomalous temperature-induced changes and all modes soften with increasing temperature. To further understand the low-temperature behavior of the crystal structure and vibrational properties of Sb_2Se_3, single-crystal data are required; however, this is out of the scope of this study.

Based on the mean force constants, total and element-specific Debye temperatures, and Grüneisen parameters, we provided a detailed analysis of the lattice dynamics of this compound. Although our theoretical approach is not suitable to accurately reproduce the measured total and partial DPS, reflected from numerical deviations between the experimentally determined and theoretically predicted values of the vibrational parameters, a proper scaling of our predicted phonon data, however, clearly shows that the observed deviations are not only due to the mismatch between the experimentally determined and theoretically predicted lattice parameters. Therefore, we conclude that the theoretical data underestimate the strength of at least some of the covalent Sb—Se bonds.
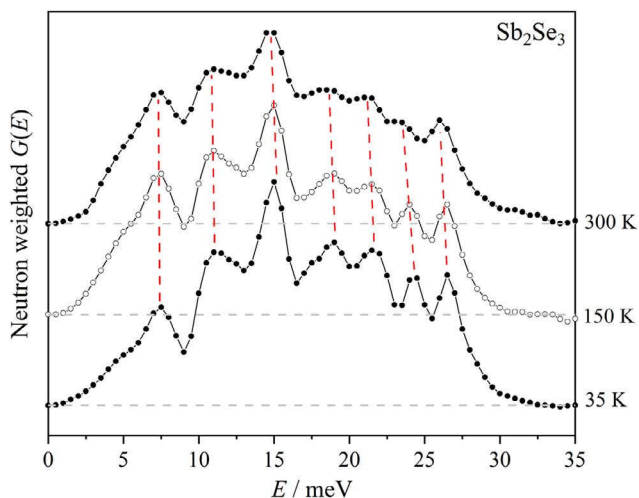
Figure 5. Temperature-induced mode shifts in the total DPS of Sb_2Se_3. The mode shifts are emphasized by dashed lines.

4. Experimental Section

For the [121]Sb NIS measurement, a polycrystalline Sb_2Se_3 sample was synthesized according to the procedure described by Herrmann et al.[9] For the INS experiments, a commercial Sb_2Se_3 sample (Sigma Aldrich, 99.999%) was used. The choice of different samples was explained because it was difficult to synthesize the amount of sample required for the INS experiment by the method presented by Herrmann et al.[9] The phase purity of both samples was confirmed by XRD measurements. The chemical composition was studied by X-ray fluorescence spectroscopy (XFS), which resulted in a composition of $Sb_{2.00(1)}Se_{3.01(1)}$ for both samples.

Low-temperature powder diffraction measurements on the NIS sample were performed using a Huber G670 Guinier Camera which was equipped with a He closed-cycle cryostat and an image plate detector (Cu Kα,1; $2\theta = 0°$–$100°$; $\Delta\theta = 0.005°$). The sample was cooled down to 40 K using a cooling rate of 5 K min^{-1}. Powder diffraction patterns of Sb_2Se_3 were collected with an exposure time of 2 h every 40 K up to 280 K and at 150 and 300 K. Between each temperature point, the temperature was raised with a rate of 5 K min^{-1} and subsequently stabilized using a dwell time of 5 min.

Le Bail refinements were performed on all powder patterns using the program JANA2006.[11] The background was described with 100 points and fitted together with the zero shift using a 20-parameter Legendre polynomial function. The peak profile was fitted with a pseudo-Voigt function including an angle-independent Lorentzian (LX) and Gaussian contribution (GW). Starting values for the lattice parameter at ambient temperature were taken from a previous study.[5]

INS experiments on Sb_2Se_3 were performed at the beamline Wide Angular-Range Chopper Spectrometer (ARCS) (Spallation Neutron Source [SNS], ORNL, TN, USA).[12] An Al can was filled with the sample in He atmosphere and then sealed with an indium ring. An empty Al can was used for background determination. Time-of-flight (TOF) spectra of Sb_2Se_3 were collected at 39, 150, and 300 K using an incident neutron energy of 45 meV. The frequencies of the T_0 chopper and of the Fermi chopper were set to 90 and 300 Hz, respectively.[12] At each temperature, data were measured twice for 1 h. The binning of the measured TOF spectra and the subsequent calculation of scattering functions was performed with the program Data Analysis and Visualization Environment (DAVE).[13] The sample scattering functions were determined by subtracting the empty can data from the measured total scattering function. In the scattering data, a Bragg peak at around 2.7–2.8 Å^{-1} was selected and the energy spectrum around this peak served as elastic line for the subsequent data treatment. The inelastic contribution was deduced by subtracting the elastic line using the program subs02 (P01, DESY). The total DPS was determined using a modified version of the program DOS.[14] For separating multiphonons, the recoil energy was set to a value of 2 meV close to the average value of $(\hbar \cdot Q)^2 / 2 \cdot m_i$ ($\hbar$: reduced Planck constant; Q: average momentum transfer; m_i: element mass) in the compound.

The [121]Sb NIS experiments were performed at the Dynamics Beamline P01 at PETRA-III (DESY, Hamburg) using a sapphire backscattering high-resolution monochromator.[15,16] The incident beam energy was adjusted to the Sb resonance (37.13 keV). About 5 mg of Sb_2Se_3 were distributed on an area of 5 × 5 mm^2 and covered by Al tape. The sample was placed in a cryostat and cooled to a temperature of 15 K to get a sufficiently high Lamb–Mössbauer factor. Using detailed thermal balances of the negative and positive parts of the spectrum evaluated with the Bose–Einstein statistics, the sample temperature was estimated to be 39(5) K. NIS spectra were measured over 8 h in several scans, which were binned and summed up. All spectra were collected with an energy resolution of around 1.4 meV. The [121]Sb partial DPS was calculated from the NIS spectrum using a modified version of the program DOS,[14] which includes a deconvolution of the NIS spectra with the instrumental function and convolution by a Gaussian function to consider the asymmetry of the instrumental function. The instrumental resolution function and the NIS spectrum of Sb_2Se_3 are shown in Figure S1, Supporting Information.

For the subsequent data treatment, both the total and partial DPS were normalized to the area between 0 meV and the cutoff energy (see later).

The Se partial DPS of Sb_2Se_3 was determined by subtracting the Sb partial DPS from the total (neutron weighted) one, using Equation (6)

$$G(E) = \frac{\sum_i n_i \cdot g_i(E) \cdot \frac{\sigma_i}{M_i}}{\sum_i n_i \cdot \frac{\sigma_i}{M_i}} \tag{6}$$

where $G(E)$ and $g(E)_i$ are the total and element/isotope-specific DPS, respectively; σ_i is the element-specific total neutron scattering cross-section (Sb: 3.90(6) barns, Se: 8.30(6) barns[17]); M_i is the element mass (Sb: 121.76 amu, Se:78.97 amu); and n_i is the fraction of the elements.

Density-functional theoretical (DFT) calculations were performed using the Vienna Ab Initio Simulation Package (VASP)[18] in the framework of the projector augmented wave method.[19] Plane-wave basis sets with kinetic energies up to 500 eV were utilized. Exchange and correlation were treated following the local density approximation (LDA).[20] It is important to mention that the LDA functional should not be used together with functional for van der Waals correction, so we avoided including such van der Waals correction on purpose. However, the theoretical approach applied in this study resulted in astonishingly good results in previous studies and was therefore also chosen here.[6,7,21] Phonon properties were computed using the Phonopy program[22] based on forces obtained by VASP using 2 × 6 × 2 super cells related to the orthorhombic Sb_2Se_3 unit cell. Total and partial densities of phonon states were computed on 8 × 24 × 8 meshes of reciprocal space points. A weighting of our theoretically predicted total and partial DPS by the element-specific neutron scattering cross sections was conducted using Equation (6). Atomic force constants were derived from the force constant matrices obtained from Phonopy as described by Stoffel et al.[7] Mode-specific Grüneisen parameters were calculated as implemented in Phonopy using 8 × 24 × 8 meshes of reciprocal space points and data obtained from the equilibrium structure and theoretically optimized structures based on scaled lattice vectors (±1%). All calculations were performed at a reference temperature of 0 K.

Conflict of Interest

The authors declare no conflict of interest.

Keywords

[1] M. Huang, P. Xu, D. Han, J. Tang, S. Chen, *ACS Appl. Mater. Interfaces* **2019**, *11*, 15564.

[2] X. Liu, C. Chen, L. Wang, J. Zhong, M. Luo, J. Chen, D.-J. Xue, D. Li, Y. Zhou, J. Tang, *Prog. Photovolt. Res. Appl.* **2015**, *23*, 1828.

[3] D. P. Gosain, T. Shimizu, M. Ohmura, M. Suzuki, T. Bando, S. Okano, *J. Mater. Sci.* **1991**, *26*, 3271.

[4] P. Arun, A. G. Vedeshwar, *Thin Solid Films* **1998**, *335*, 270.

[5] G. P. Voutsas, A. G. Papazoglou, P. J. Rentzeperis, D. Siapkas, *Z. Kristallogr.* **1985**, *171*, 261.

[6] V. L. Deringer, R. P. Stoffel, M. Wuttig, R. Dronskowski, *Chem. Sci.* **2015**, *6*, 5255.

[7] R. P. Stoffel, V. L. Deringer, R. E. Simon, R. P. Hermann, R. Dronskowski, *J. Phys.: Condens. Matter* **2015**, *27*, 085402.

[8] Y. Liu, K. T. E. Chua, T. C. Sum, C. K. Gan, *Phys. Chem. Chem. Phys.* **2014**, *16*, 345.

[9] M. G. Herrmann, R. P. Stoffel, R. Dronskowski, K. Friese, *J. Phys.: Condens. Matter* **2018**, *30*, 405702.

[10] P. Hofmann, *Solid State Physics*, Wiley-VCH, Weinheim, Germany **2015**.

[11] V. Petricek, M. Dusek, L. Palatinus, *Z. Kristallogr.* **2004**, *229*, 345.

[12] D. L. Abernathy, M. B. Stone, M. J. Loguillo, M. S. Lucas, O. Delaire, X. Tang, J. Y. Y. Lin, B. Fultz, *Rev. Sci. Instrum.* **2012**, *83*, 015114.

[13] R. T. Azuah, L. R. Kneller, Y. Qiu, P. L. W. Tregenna-Piggott, C. M. Brown, J. R. D. Copley, R. M. Dimeo, *J. Res. Natl. Inst. Stand. Technol.* **2009**, *114*, 341.

[14] V. G. Kohn, A. I. Chumakov, *Hyperfine Interact.* **2000**, *125*, 205.

[15] P. Alexeev, V. Asadchikov, D. Bessas, A. Butashin, D. Deryabin, F.-U. Dill, A. Ehnes, M. Herlitschke, R. P. Hermann, A. Jafari, I. Prokhorov, B. Roshchin, R. Röhlsberger, K. Schlage, I. Sergueev, A. Siemens, H.-C. Wille, *Hyperfine Interact.* **2016**, *237*, 59.

[16] I. Sergueev, H.-C. Wille, R. P. Hermann, D. Bessas, Y. V. Shvyd´ko, M. Zajac, R. Rüffer, *J. Synchr. Rad.* **2011**, *18*, 802.

[17] V. F. Sears, *Neutrons News* **1992**, *3*, 26.

[18] G. Kresse, J. Furthmüller, *Comput. Mater. Sci.* **1996**, *6*, 15.

[19] P. E. Blöchl, *Phys. Rev. B* **1994**, *50*, 17953.

[20] J. P. Perdew, A. Zunger, *Phys. Rev. B* **1981**, *23*, 5048.

[21] A. F. Zurhelle, V. L. Deringer, R. P. Stoffel, R. Dronskowski, *J. Phys.: Condens. Matter* **2016**, *28*, 115401.

[22] A. Togo, I. Tanaka, *Scr. Mater.* **2015**, *108*, 1.